M. Babič

Faculty of Information Studies
University of Novo Mesto
Novo Mesto
Slovenia

P. Wangyao

Department of Metallurgical Engineering
Chulalongkorn University, Bangkok
Thailand

B. Šter

Faculty of Computer and Information
Science, University of Ljubljana
Ljubljana
Slovenia

D. Marinković

Department of Structural Analysis,
TU Berlin
Berlin
Germany

C. Fragassa

Department of Industrial Engineering, Alma
Mater Studiorum University of Bologna
Bologna
Italy

Modelling the Surface Roughness of Steel after Laser hardening by using 2D Visibility Network, Convolutional neural Networks and Genetic Programming

The surface characterization of materials after Robot Laser Hardening (RLH) is a technically demanding procedure. RLH is commonly used to harden parts, especially when subject to wear. By changing their surface properties, this treatment can offer several benefits such as lower costs for additional machining, no use of cooling agents or chemicals, high flexibility, local hardening, minimal deformation, high accuracy, and automated and integrated process in the production process. However, the surface roughness strongly depends on the heat treatment and parameters used in the process. This article used a network theory approach (i.e., the visibility network in 2D space) to analyze the surface roughness of tool steel EN100083-1 upon RLH. Specifically, two intelligent methods were merged in this investigation. Firstly, a genetic algorithm was applied to derive a relationship between the parameters of the robot laser cell and topological surface properties. Furthermore, convolutional neural networks allowed the assessment of surface roughness based on 2D photographic images.

Keywords: *Robot Laser Hardening (RLH); Roughness, Genetic Algorithm; 2D Visibility Network; Convolutional Neural Networks.*

1. INTRODUCTION

Laser Hardening is a surface heat treatment that can significantly increase the hardness of steel parts [1]. This is essential, for instance, when high wear resistance is required to provide proper functional properties. Unlike the well-known thermal hardening processes, such as volumetric quenching, high-frequency currents, electric heating, quenching from the melt, and other methods, laser hardening is not a volumetric but a local, surface process, which excludes changes in both the macro and micro-geometry of the workpieces.
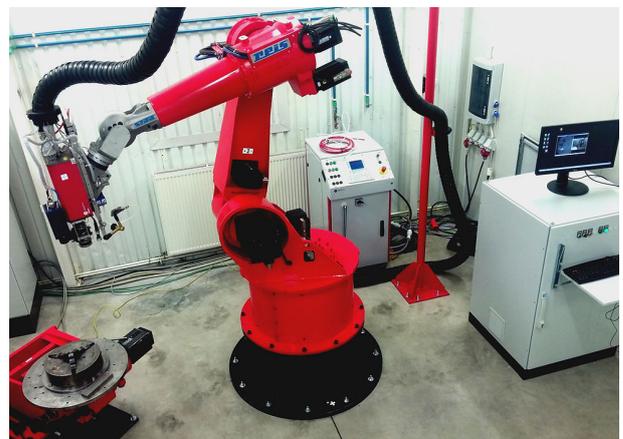
It is a very cost-effective and extremely fast hardening procedure, especially convenient for large parts made by metal forming technology. In this case, it allows the precise hardening of the outermost layers irradiating limited portions on the surface. While the laser beam highly localizes the heat on the surface, the core remains in its original state: the less heat is generated, the less distortion occurs in part [2].

Under the laser beam, martensite is created: a very hard and fine metal structure responsible for improving the material hardness. Using laser hardening, it is possible to locally harden the laser-irradiated area, handling irregular and three-dimensional workpieces and avoiding unnecessary rework and missed work [3].

When a robot moves the laser beam, the process is

called Robot Laser Hardening (or RLH). This process offers additional advantages (accuracy, speed, energy efficiency, etc.) over other traditional heat treatments emerging. It was verified by one of the authors, e.g., that RLH can increase material hardening at a depth of 0.8-1.5 mm, significantly improving wear resistance and service life with an extra cost not exceeding 15-20% [4].

Fig. 1 shows a robot laser cell for metal hardening, as available in the laboratory for experiments. Using this equipment, it was possible to harden metal specimens in the present investigation according to different process parameters.

Fig. 1: Robot laser cell for hardening.

RLH is carried out without melting the surface, thus eliminating a modification in roughness and the need for subsequent machining (e.g., grinding, polishing, etc.). Furthermore, the possibility of hardening and modifying surfaces in the case of a wide range of materials with a

significant increase in their performance characteristics allows, in many cases replacing expensive, complex-alloyed materials often used to ensure the necessary wear resistance of surfaces with simpler, cheaper, and more affordable ones, giving (additionally) them the desired performance characteristics.

The thermal cycle proposed by the RLH is the fastest compared to the thermal cycles of every other existing hardening method. These conditions provide a high rate of heating and cooling of the treated surface areas, as a result of which certain effects are achieved, such as high surface hardness, high dispersion, and uniformity of the structure, a decrease in the friction coefficient, an increase in the bearing capacity of the surface layers. In addition, no problems are noticed with the bond strength (adhesion) of the hardened layer with the bulk of the part, which is typical, for instance, for spraying technology.

Finally, the modern RLH equipment offers the chance of hardening surfaces of any complexity and geometry, with direct effects on productivity. The evident high productivity of this technology is due to the automation of the RLH process and the elimination of the need for heat treatment of the entire part: only local areas subject to wear are treated. Using a local treatment and a small amount of heat, as permitted by RLH, minimizes the thermal deformation while quick cooling enables a robust microstructure [5].

The present paper aims to analyze and predict the topographical property and roughness of RLH specimens. With the scope, *visibility graphs* were used.

A graph is a mathematical object that has proved helpful in many theoretical and applicative situations [6]. One way graphs are commonly represented in a 2D plane, or a 3D space is the so-called *visibility repr–esentation,* where nodes represent disjunctive objects, and a connection exists between them when one "sees" the other. A visibility graph (or network) is a graph of inter-visible locations, typically for a set of points and obstacles in the Euclidean plane. A visibility graph is a kind of graph where each edge incident to a vertex shows the direction of the other visible vertices.

In the present analysis, visibility graphs are adopted to transform RLH surfaces into schemes, while several parameters, specifically created with the scope to classify graphs, are used to detect these schemes, transforming them into numbers and factors. Then, two *intelligent systems* (IS) were considered and compared as advanced tools for data mining.

An IS can be considered a sophisticated algorithm able to solve complex tasks, even without all the needed information, thanks to unpredictable operational modes, more like a form of artificial intelligence than a rational evaluation [7].

The use of IS is consolidated as a way for material properties prediction, including several investigations proposed by authors in the years. For instance, in [8], a neural network was used to calculate the tensile strength of aluminum-silicon carbide starting from acoustic emission rise angle data. At the same time, in [9], the prediction was focused on the tensile behavior of cast alloys and performed by a pattern recognition analysis. Regarding the hardness and roughness, both [10] and

[11], together with the already mentioned [4], can represent a preliminary analysis able to confirm the goodness of IS methods in performing evaluations and predictions.

With that scope, it is useful to recall a few common surface roughness concepts. The roughness refers to the surface micro-geometry and is considered in small areas (up to several square millimeters). It can be considered a combination of surface irregularities with relatively small steps, highlighted using the base length.

In this paper, differently from the previous ones, a new approach to intelligent recognition of surface roughness based on graph theory and intelligent systems (IS) was developed and used to investigate its dependence on RLH process parameters [10]. Specifically, concerning the extremely long list of IS, due to previous positive experiences, we preferred:

- Convolutional neural networks (CNNs) represent a special typology of artificial neural networks (ANN), based on translation-invariant local feature detectors or filters, which share their adaptable parameters (*weights*) [12, 13]. In these networks, a convolution layer is often followed by a pooling layer, which compresses information, usually by maximizing or averaging rectangular areas of pixels, thus effectively reducing large amounts of image data. Convolution and pooling layers can be reapplied several times to further reduce data consistency. The output of the last layer (*output*) predicts target variables, in our case, the surface roughness.
- Genetic programming (GP) is one of the most efficient and universal methods for solving problems developers use to face [14-16], such as symbolic regression, data mining, design optimization [17], and research of the behavior of developing populations (emergent behavior) in biological communities. GP belongs to a class of methods known as evolutionary algorithms since they are based on the concepts of natural selection and evolution (as evident in [18]).

2. MATERIALS AND METHODS

2.1 Materials preparation

In this paper, we present a new approach for modeling the surface roughness of materials by using a 2D visibility network, convolutional neural networks, and genetic programming.

The hardening process was performed by standard tool steel EN $100083 - 1$ using the robot laser cell, RV60-40 (Reis Robotics Company), with a power of 1500 W with modification on
- speed in the range v $\in$ [2, 5] mm/s
- the temperature in the range T $\in$ [1000, 1400] °C.

Surface characterization, performed by profilometry techniques, yields information on the roughness. Specifically, according to the scheme in Fig. 2, the surface roughness was conveniently characterized considering the surface profile (Z(x)) with respect to an arithmetic/baseline by the following parameters:
- R_a, as average deviation on a typical length (lr),
- R_z, as the maximum height of the profile roughness,

- R_p, as maximum profile peak height,
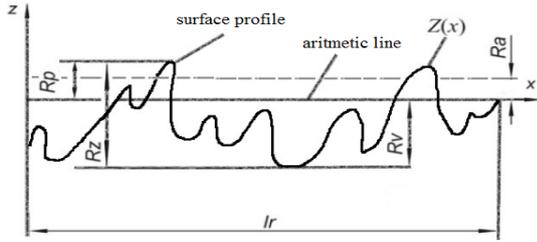- R_v, as maximum profile valley depth.

Fig. 2: Surface roughness and main parameter.

Fig. 3 depicts the surface roughness material of RLH with 2 mm/s at 1400 °C. On the right-hand side, an arrow shows the direction of traveling of the laser beam. On the left, we can see a profile graph of the roughness of the robot laser hardened specimen with 2 mm/s at 1400 °C. Ra_0 represents the initial roughness before hardening, and Ra represents roughness after the RLH treatment.
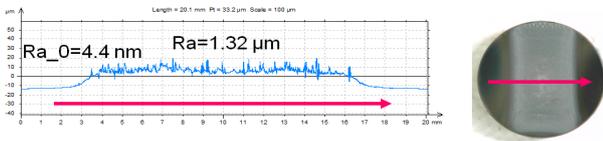

Fig. 3: RLH surface roughness with 2 mm/s at 1400 °C.

2.2 Methodology

We use the network theory, especially the concepts related to the visibility network, with the scope to analyze the surface roughness. The nodes of a visibility graph correspond to geometric components, such as vertices or edges. An edge of the graph connects two nodes if the components can "see" each other, perhaps under some restricted form of visibility. Two nodes of a 2D graph with values (x_a, y_a) and (x_b, y_b) will have visibility and consequently will become two connected nodes of the associated graph, if any other data (x_c, y_c) placed between them fulfil [19]:

$$y_c < y_b + (y_a - y_b) \times (x_c - x_b)/(x_a - x_b) \qquad (1)$$

Fig. 4 represents an example of a visibility graph in 2D space. Red color lines indicate connections between the points that have visibility. The green line (virtual) represents the situation where inequality in equation (1) is not gathered.
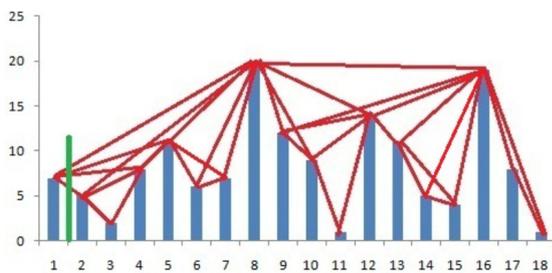

Fig. 4: Example of a visibility graph in 2D space.

First, we find coordinates (x,y) of the surface roughness of the RLH specimen from the graph in Fig. 3. Then, we use the algorithm for visibility networks in 2D space. After this, we modify the network from a linear network to a 2D network – a 2D surface network.

The last step is calculating the topological properties of the surface network. For calculating the topological properties, we use the Pajek program (as done in [20]). We calculated and used the three topological properties: 1) triadic census type 16 – 21C; 2) Average Degree; 3) All Degree Centralization.

For mathematical modeling, we use genetic programming (GP) to find the relationship between parameters of robot laser cells and topological properties of visibility networks of surface roughness of hardened materials. Fig. 5 shows an example of the application of the GP method. On the left side, we can see the GP tree, and on the right side is the tree's mathematical equation. Specifically, we use the following GP attributes, which proved to provide the best results in terms of prediction of the RLH specimen's roughness:

- size of the population of organisms: 500
- maximum number of generations: 100
- reproduction probability: 0.5
- crossover probability: 0.7
- maximum permissible depth in the creation of the population: 7
- maximum permissible depth after the operation of crossover of two organisms: 10
- smallest permissible depth of organisms in generating new organisms: 2
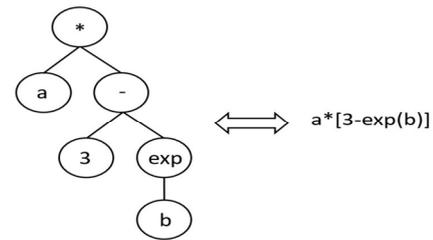- tournament size used for selection of organisms: 6.

Fig. 5: An example of genetic programming.

It is reasonable to assume that the speed and tempe–rature of laser hardening strongly impact roughness [21]. We were interested in checking if the specimens' images would contribute to the evaluation of surface roughness and confirm the assumption mentioned above.

Specifically, Fig. 6 represents the five-step proce–dure applied with the scope to determine the topological properties of RLH surfaces: starting from images taken from RLH specimens, we used the visibility net–work method to convert them into 2D graphs and to evaluate their topological properties (i.e., triadic census type…).

Then, topological data was used with respect to two different methods: without or directly integrating images.

In the first case, an ordinary multilayer perceptron was applied to predict roughness from two inputs: speed and temperature. In the second case, a convolutional neural network (CNN) was applied, as shown in Fig. 7. The CNN was trained by combining the process para–meters (temperature and speed) with information from the digital micrograph analysis. During the training phase, CNN weights were set to reduce the prediction error. Due to the fact that images present complex information to be stratified and classified, CNNs typically include multiple convolution layers, followed by *pooling operations* to gradually reduce the amount of data [22]. This directly opens the way to the concepts of deep learning.
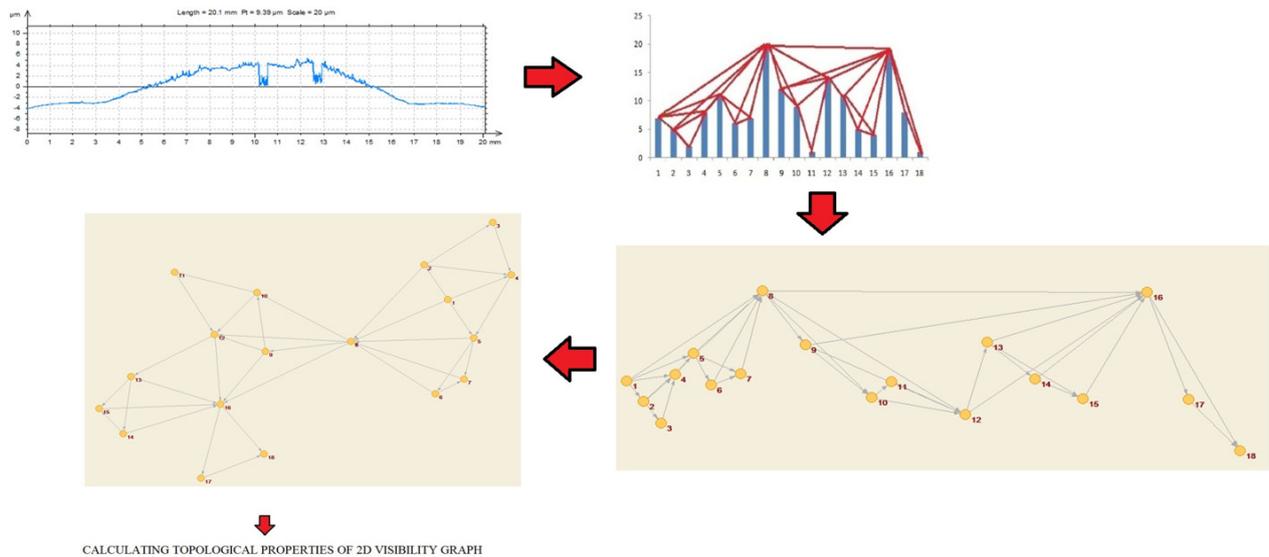
Fig. 6: Process of calculating topological properties of surface roughness of RLH specimens.
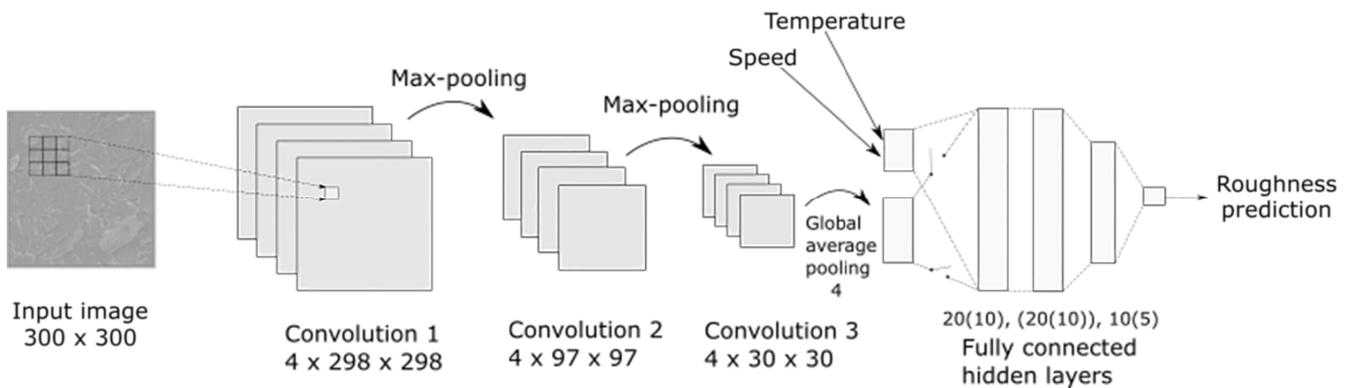

Fig. 7: Convolutional neural network. In the first approach (without images), the global average pooling layer is not connected to fully connected layers, while it is connected in the second approach (with pictures).

The Spearman correlation coefficient (ρ) verified the relationship between the variables. Also called linear correlation coefficient, this statistical index highlights a linear relationship between variables. It can be used to provide a statistical measure of the strength of a monotonal link between data pairs. This coefficient can also be applied to rank the existing relationship between different series of indicators (e.g., in [9]). We used the Spearman correlation coefficient *(ρ)* to weigh and compare the existing correlations between measures and predictions regarding both IS.

The non-dimensional ρ can present values $\in [-1, 1]$, and closer the connection to one, the stronger the monotonic connection is, as:

ρ = 0.00	no correlation
0.01 <ρ <0.19	slight correlation
0.20 <ρ <0.39	low / weak correlation
0.40 <ρ <0.59	medium / moderate correlation
0.60 <ρ <0.79	high / strong correlation
0.80 <ρ <1.00	very high /very strong correlation

3. RESULTS

With respect to N. 21 specimens under investigation, namely, from S1 to S21, Table 1 summarizes the RLH process parameters impacting roughness (as temperature and speed), together with the topological parameters as detected by the analysis.

Specifically, regarding the:
- process parameters: P_1 and P_2 represent, respect–tively, the temperature [°C] and speed [mm/s] of the laser beam during the RLH process, while Ra is the measured roughness [nm].
- Topological properties: X_1 represents the triadic census type $16 - 21$, X_2 is the Average Degree, and X_3 is the number of extremes.

Entering in detail about specimens and experiments,
- S_{21} represents the specimen before the process of RLH and can be used as the basis for all considerations.
- Specimens from *S*1 to *S*8 were hardened with v $\in$ [2-5] mm/s and T$\in$[1000-1400] °C: such parameters were chosen according to conventional applications of RLH.
- In specimens from *S*9 to *S*16, the hardening process was repeated with the same parameters to investigate the effect of a double treatment.
- Among these specimens, the *S*13 exhibits the highest roughness (2350 nm) rather due to the very high temperature and low speed of processing
- Specimens from *S*17-*S*21 faced an on-the-spot RLH process: the laser beam's speed was zero.

Table 1. RLH process parameters, roughness (*Ra), and topological properties.*

Sample	Process parameters		Roughness	Topological properties		
	P_1 (°C)	P_2 (mm/s)	*Ra* (nm)	X_1	X_2	X_3
S1	1000	2	201	486562	6.68	120823
S2	1000	3	171	419143	6.31	125787
S3	1000	4	109	426718	6.36	123943
S4	1000	5	76	435387	6.40	124833
S5	1400	2	1320	421225	6.32	124626
S6	1400	3	992	379602	6.08	131540
S7	1400	4	553	419628	6.32	126962
S8	1400	5	652	374160	6.05	130799
S9	1000	2	337	425656	6.40	123393
S10	1000	3	307	448399	6.46	126395
S11	1000	4	444	420703	6.32	124296
S12	1000	5	270	435387	6.40	123829
S13	1400	2	2350	486206	6.58	128143
S14	1400	3	1900	587747	7.03	122500
S15	1400	4	661	419975	6.37	120818
S16	1400	5	759	584852	7.12	116812
S17	800	0	183	377479	6.06	133031
S18	1400	0	1330	381919	6.07	130974
S19	2000	0	1740	374666	6.05	131043
S20	950	0	502	728408	7.92	95090
S21	850	0	166	176414	10.8	106916

This collection of data was used for performing the analysis and prediction of roughness.

In Table 2, a comparison between the actual and pre–dicted roughness is presented. Specifically, *Ra* provides the value of roughness as measures *(Y)*, while GP and CNN are estimations obtained from genetic programming and convolutional neural network models, respectively.

Percentual errors are also reported per each measure, with average errors of -42% (i.e., underestimation) and 20% (i.e., overestimation) in the case of, respectively, GP and CNN. It is immediately evident that, except in some points where the errors are very high, there is a good general correspondence between the measures and the predictions.

Table 2. Actual and predicted (by genetic programming and convolutional neural network models) values of roughness.

S	*Y*	GP	CNN	$err^{\%}_{GP}$	$err^{\%}_{CNN}$
S1	201.0	190.2	310.60	-5%	55%
S2	171.0	175.8	190.05	3%	11%
S3	109.0	100.9	200.53	-7%	84%
S4	76.0	80.6	315.32	6%	315%
S5	1320.0	233.3	1221.44	-82%	-7%
S6	992.0	202.1	1021.39	-80%	3%
S7	553.0	57.4	683.58	-90%	24%
S8	652.0	93.1	539.16	-86%	-17%
S9	337.0	313.3	231.40	-7%	-31%
S10	307.0	257.3	213.14	-16%	-31%
S11	444.0	324.7	191.03	-27%	-57%
S12	270.0	80.6	240.58	-70%	-11%
S13	2350.0	181.3	1175.04	-92%	-50%
S14	1900.0	1726.6	1340.49	-9%	-29%
S15	661.0	222.9	742.89	-66%	12%
S16	759.0	410.2	681.45	-46%	-10%
S17	183.0	200.0	148.44	9%	-19%
S18	1330.0	189.3	1396.80	-86%	5%
S19	1740.0	193.3	1776.57	-89%	2%
S20	502.0	265.5	518.99	-47%	3%
S21	166.0	158.0	441.77	-5%0	171%

In the case of the GP model, the relation between roughness (*Ra* in Table 2) and Topological properties (X_1, X_2, X_3 in Table 1) is given by Eq. 2 (where *Ra* is named as *Y*):

$$
\begin{aligned}
&Y \\
&= X_3\Bigg(2X_1 - \frac{5.94731 X_3 X_1}{7.68826 + X_3} \\
&\quad -1.87432 + \frac{X_2 + 0.168143\,(26.185 + X_2)}{X_3} \\
&\quad + \frac{X_3 - \frac{X_1 X_3}{7.68826}}{} \\
&\quad + \frac{X_1\left(-X_2 + \frac{X_1 X_3}{7.68826 + X_2}\right)}{X_2{}^2 + \left(\frac{200153}{X_3} + 0.214435 X_1 X_3\right)\left(-5.25683 + \frac{X_1 X_3}{7.68826}\right)} \\
&\quad + \frac{0.20213 X_1{}^2 X_3}{X_2\left(X_2 + X_3 + \frac{0.773557 X_1 X_3}{X_2 + \frac{X_1 X_3}{7.68826 + 5.94731 X_2}}\right)} \\
&\quad + \frac{X_2{}^2 + \frac{X_1 + X_2}{\left(12.3517 + \frac{0.200153}{X_3}\right)\left(-5.25683 + \frac{X_1 X_3}{7.68826 + X_3}\right)}}{-1.87423 + \frac{}{-X_2 + \frac{X_1 X_3}{X_2 - X_3}}} \\
&\quad - (X_1 - X_2) \\
&\quad + \frac{X_2 + 0.168143(26.185 + X_2)}{X_3} \\
&\bigg/\bigg((7.68826 + X_3 \\
&\quad - \frac{X_1 X_3}{7.68826 + X_2 + 0.363765(-X_1 + X_2)X_3{}^2}\bigg) \\
&\quad \times \bigg(-4.66342 \\
&\quad - X_2 + \frac{X_1 X_3}{X_2 - 5.94731 X_3} \\
&\quad - \frac{0.20213 X_1 X_3\left(-2.61271 + \frac{X_2 + \frac{X_1 X_2}{7.68826 + X_2 + 5.94731 X_3}}{X_3}\right)}{(-1.87432 + X_1)X_2}\bigg)\bigg)\Bigg)
\end{aligned}
\tag{2}
$$

In Fig. 8, values from Table 2 are also graphically displayed, highlighting a clear match in most situations. Specifically, Y represents the measured data while red and green points represent predictions from GP and CNN. Finally, in Fig. 9, it is possible to find examples of micrographs (for specimens S1 to S4, three images each) used as additional inputs to reinforce CNN's predictions. These specimens are different because they are treated by an RLH process characterized by the same source temperature (1000 °C) but different speeds (2, 3, 4, and 5 mm/s).
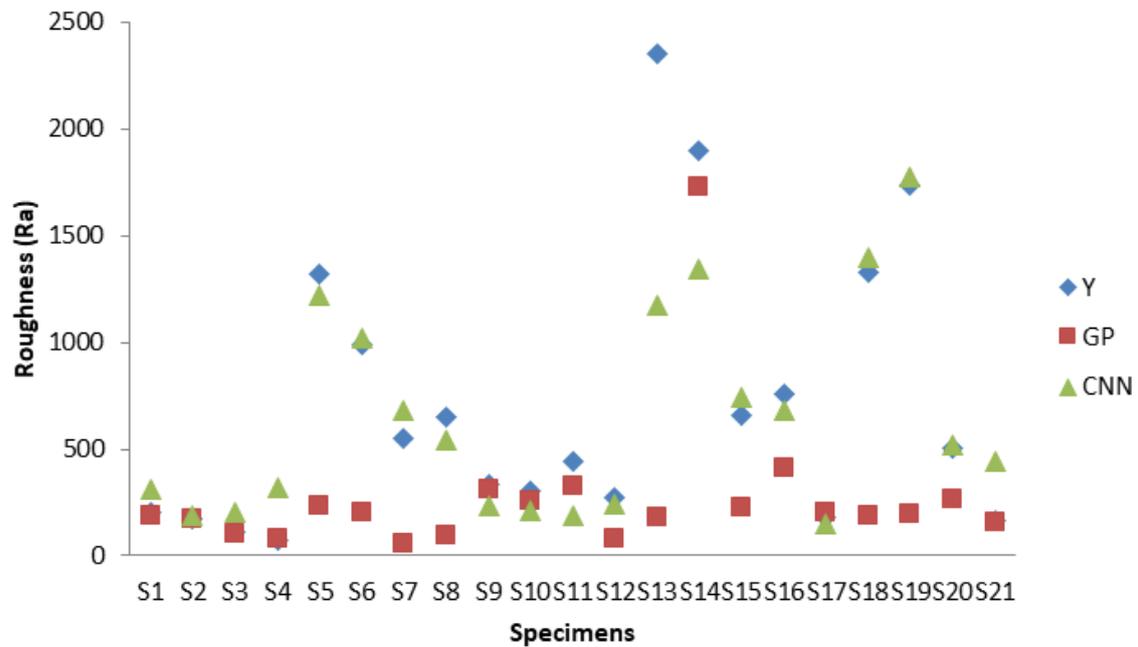
Fig. 8: Measured (Y) and predicted surface roughness, according to Genetic Programming (GP) and Convolutional Neural Network (CNN).
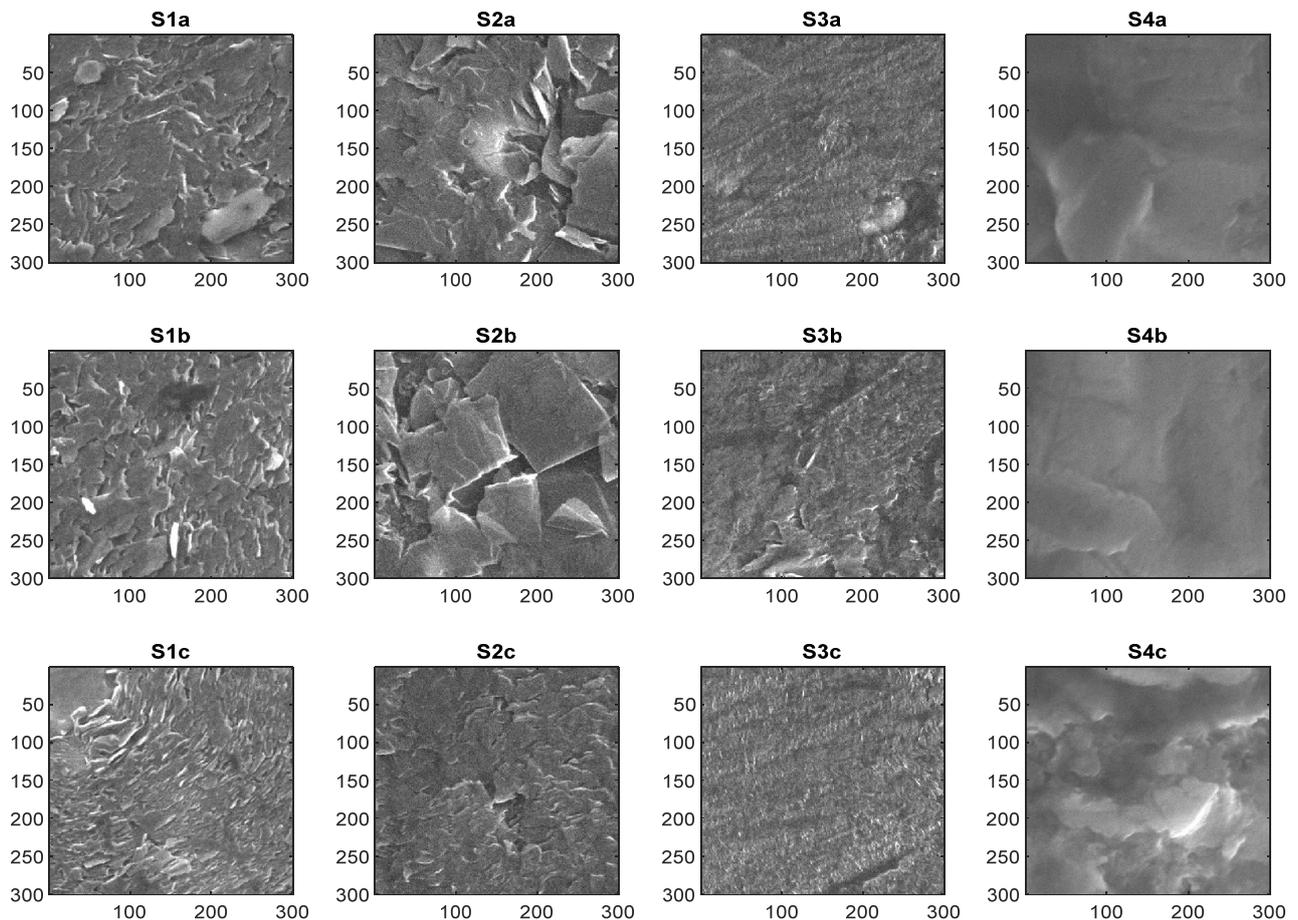

Fig. 9: Micrographs of specimens characterized by a speed treatment of 2 (S1), 3 (S2), 3 (S3), and 5 mm/s (S4) (at 1000 °C).

4. DISCUSSION

The surface roughness of an RLH hardened material significantly influences the macroscopic contact angle measurement on its flat surface, with significant effects in terms of industrial applications. E.g., it affects the tribological behavior of surfaces. The surface roughness can quickly increase friction and inefficiencies.

Our objective was to investigate how the RLH process (i.e., speed and temperature) affects surface roughness and can be optimized. With such a scope, three tools were merged:

Visibility network analysis

It would be worthwhile to analyze the graph of roughness surface with the network theory, especially visibility net–work in 2D space. It can be shown that the method of visi–bility graph is very useful for researching the surface roughness of materials after the RLH process. Some rem–arks: specimen S20 has the highest topological pr–operty triadic census type 16 – 21; specimen S21 has higher topological property Average Degree and speci–men; S17 has a higher topological property number of extremes; specimen S21 has the lowest topological pro–perty triadic census type 16 – 21; specimen S8 has the lowest topological property Average Degree, and speci–men S20 has the lowest topological property number of extremes.

Genetic programming analysis

The genetic programming (GP) was used to model the surface roughness Ra with topological property triadic census type 16 – 21, Average Degree, and several extremes of visibility graph of surface roughness *Ra*. The genetic programming model yields a deviation of 42,21% compared to the measured data. Hence, the parameter number of extremes of the surface roughness *visibility gra*ph has a higher impact on the model.

The in-house GP system was run 100 times in order to develop 100 different predictions according to the different parameters used in the robot laser cell. Each run lasted approximately two and a half hours on an I7 Intel processor and 8 GB of RAM. An in-house genetic programming system, coded in AutoLISP, which is integrated into AutoCAD, was used to obtain 100 independent models for predicting electric energy consumption during the EAF operation.

For the model fitness, the average square of deviation from the monitored data was selected. It is defined as (3):

$$\Delta = \Sigma \Delta_i^2 / n \tag{3}$$

where *n* is the size of the monitored data, and *i* is the square of deviation of a single sample data.

The deviation of a single sample data produced by an individual organism is simply (4):

$$\Delta i = E_i - G_i \tag{4}$$

where *Ei* and *Gi* are the actual and the predicted scrap fractions (which depend only on surface defects), respectively.

Convolutional neural network analysis

The convolutional neural network (CNN) was successfully used to predict the surface roughness, considering images from the surface. When images were also used, the mean squared error dropped from 0.020 ± 0.002 to 0.014 ± 0.001. This corresponds to the root mean squares of 0.141 ± 0.045 vs. 0.118 ± 0.032. Using a t-test to compare the means, $t = 0.023/0.017 = 1.35$ at 16 degrees of freedom yields the p-value of 0.18, which means that the prediction using images is signi–ficantly better than without images, at least at the given significance level.

For the experiment with the CNN, each specimen had three photos, also indicated by a, b, and c (Fig. 9 shows only specimens S1 to S4). It can be observed that, while the hardening speed increases linearly (S1: 2mm/s, S2: 3mm/s, S3: 4mm/s, S4: 5mm/s), the roughness of the surface *Ra* decreases: S1: 201nm, S2: 171nm, S3: 109nm, S4: 76nm, see Table 1. We hypothesized that a CNN would distinguish different levels of roughness from photos. The images of specimens were cropped to a uniform size of 300×300. Since they were in grayscale, only one channel was required. The values were scaled from the [0, 255] interval to the [0, 1] interval. Next, a two-dimensional convolution layer of filter size 3×3 with 4 kernels was applied, followed by a two-dimensional max-pooling (3×3) to compress the image size. The combination of 2D conv-layer and max-poling was repeated to achieve further compression. This is followed by the third conv-layer and an average pooling layer, whose output was flattened to merge with the non-image data. The CNNs were trained for 1000 epochs with the RMSprop learning algorithm with a learning rate of 0.001. The mean squared error (MSE) was recorded for both evaluated cases: without and with images. For each setting, eight different training settings were used: with two and three hidden layers, with two different sizes of layers (i.e., number of artificial neurons), and with two different activation functions of neurons (sigmoid vs. relu). The output neuron was used to predict the surface roughness. Its activation function was sigmoid in all cases. The results are given in Table 3. For each training, the result is the mean of 10 runs, with the standard deviation. Two of the three images for each parameter set (speed, temperature) were used for training and the third for testing. Therefore, we also have test results in the 'image' setting. Note that in the 'no-image' setting, testing would give the same results as training, so only training results are given.

Table 3. Roughness prediction errors (the mean squared error, MSE) using CNN in both settings: without and images.

Hidden layers	Size of layers	Activation function	Without images	With images	
			train / test	train	test
2	20, 10	sigmoid	0.023 ± 0.001	0.020 ± 0.002	0.021 ± 0.002
		relu	0.023 ± 0.002	0.016 ± 0.002	0.016 ± 0.002
	10,5	sigmoid	0.028 ± 0.001	0.027 ± 0.004	0.029 ± 0.004
		relu	0.024 ± 0.003	0.020 ± 0.004	0.021 ± 0.004
3	20, 20, 10	sigmoid	0.022 ± 0.001	0.018 ± 0.002	0.020 ± 0.002
		relu	**0.020 ± 0.002**	**0.014 ± 0.001**	**0.014 ± 0.001**
	10,10,5	sigmoid	0.027 ± 0.001	0.027 ± 0.003	0.028 ± 0.002
		relu	0.024 ± 0.004	0.020 ± 0.005	0.021 ± 0.005

Mean Values and Variability

In Table 4, the roughness surface of RLH specimens is reported as predicted by the GP and CNN in terms of mean values and standard deviations. We can see how the prediction variability is in line with the initial
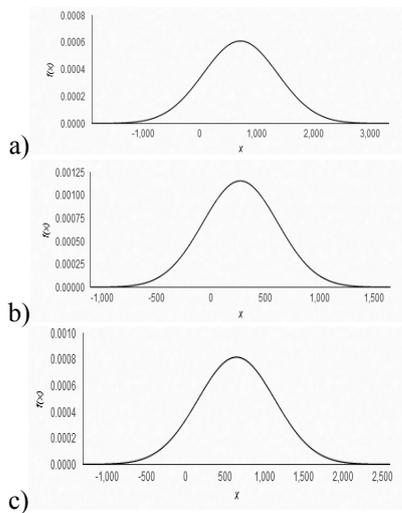
variability of measures. Measured data have the average Ra of 715 with σ=±62 (0,86%). The prediction methods GP and CNN give the average Ra of 715±62 (0,86%), 269±75 (0,7%), and 646±158 (1%).

Table 4. Ra prediction in terms of mean values and standard deviations.

Unit	Data	GP	CNN
Ra	715±62 (0,86%)	269±75 (0,7%)	646±158 (1%)

Mean Values and Error Estimation

Variabilities and errors are intrinsic to predictions and measures. It is possible to determine such aspects concerning the estimation of mean values. Specifically, Figs. 10 presents data in terms of density functions for measures and predictions. Their differences are evident.

Fig. 10: Data in terms of density function for measures and GP and CNN predictions: a) measures; b) GP predictions; c) CNN predictions.

Correlation analysis

The Spearman coefficient (ρ) was used to correlate measures and predictions (Tab. 5). Predictions are precise (and models efficient) when a linear correlation between them exists, and ρ is close to 1.

Specifically, GP cannot be considered a valid estimator with a $\rho = 0.395$ that shows a low/weak linear correlation between predictions and data.

On the contrary, with $\rho = 0.842$, CNN demonstrated the ability to provide a very high/strong correlation between predictions and measures.

Fig. 11 reports such information in graphs to exhibit the linear correlation offered by CNN (down) against the weak correlation of GP (up).
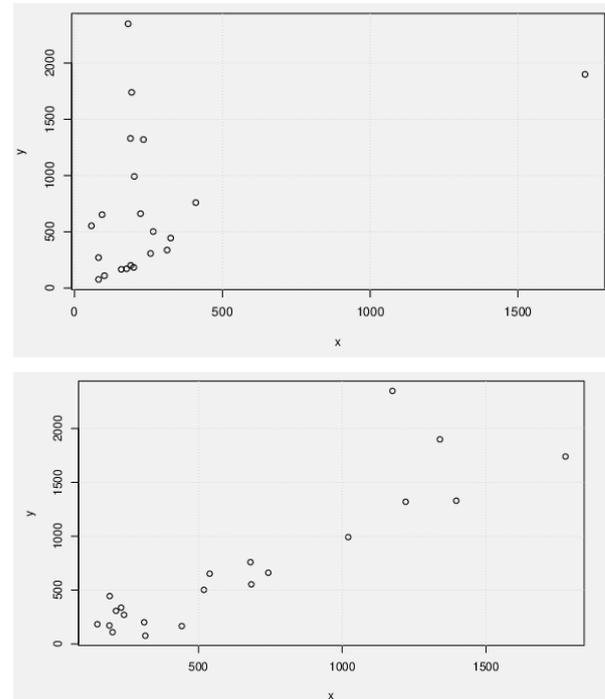
Table 5. Correlation analysis by Spearman coefficient (ρ).

Model	ρ	Correlation
GP	0.395	low/weak
CNN	0.842	very high/strong

Comparison results with previous work

With respect to previous authors' works [as 4, 9-11], a new approach to pattern recognition embedding the graph theory is proposed here. This approach was developed with the precise scope to determine the material surface roughness when depending on the process parameters of the RLH cell. The proposed method allows identifying existing relationships bet–ween the manufacturing parameters and microstructural features as directly detected by micrographs. Similarly, with respect to other past studies, methods coming from the network theory were used here, but these methods are different in their applications. For instance, in [11], also referable to the surface characterization of tool steel, thermally treated by RLH, the structural complexity of materials was determined using fractals (instead of graph theory). Moreover, this is the first time that topological properties such as triadic census type16 – 21, average degree, and the number of extremes of the visibility network are used to investigate RLH.

Fig. 11: A graphical representation of linear correlation for GP (up) and CNN (down) predictions.

5. CONCLUSION

In this work, the robot laser hardening (RLH) surface treatment was investigated with the scope of predicting the roughness with respect to different process para–meters (i.e., temperature and speed of laser beam). RLH is a special surface heat treatment that offers several benefits (e.g., it does not require re-machining). This technique is applied for hardening precisely defined areas like high-stressed radii, areas in molding plates, coining steels, cutting edges on draw die punches, and lower die. The possibility of automating the process makes the ability to predict its results very interesting.

Micrographs are permitted to distinguish the effect of hardening on the surfaces. Specifically, 21 specimens (in steel) were manufactured using robot laser cells for hardening with respect to different process conditions. Using concepts as visibility graphs in 2D space, the topographical properties of the roughness after RLH were evaluated. Genetic programming (GP) and

convolutional neural networks (CNN) were then used with the scope to recognize patterns in data. Several relations between process parameters and material characteristics emerged. A good correlation between predictions and measures was evident (in the case of CNN), confirming the possibility of using intelligent systems to investigate material problems.

The main findings and outcomes can be summarized as follows:

- a new approach was developed and validated with the scope to analyze the effects of RLH on the sur–face roughness of materials.
- Laser beam speed and temperature can be conve–niently selected as process parameters for such a scope.
- An approach based on the visibility network and visibility graphs was demonstrated as efficient in the surface analysis.
- The surface roughness graphs were converted to a 2D surface network permitting extrapolating of their topological properties.
- Intelligent systems, i.e., genetic programming and convolutional neural network, were helpful in pattern recognition and data mining.
- *Ra* prediction was presented in terms of the mean values and standard deviations.
- Measured and predictions can be considered in terms of the density function.
- Spearman linearity was effective in evaluating accuracy in predictions.

6. FUTURE WORK

In RLH, a relevant problem, not properly investigated at the moment, is related to the fact that it is very hard to process geometrically complex parts as sprockets. The possibility of predicting the effect of RLH by effective intelligent systems (as here investigated) opens the doors to developing more complex processes and RLH plants.

In particular, as the next step, we intend to enlarge the current results to a robot laser cell specifically developed to solve the problem of hardening sprockets and other similar parts. These new systems will be based on the ability to use two laser beams during the RLH simultaneously: a prism will divide the laser beam in two (Fig. 12). It could represent innovative equipment in line with the recent process of such a research field [23, 24]. In the future, we want to explore how different parameters of a laser beam in this 'tandem process' can affect the properties of the material (roughness), investigating general aspects of the new process as:

- point two laser-beam hardenings,
- two laser-beam hardening with overlapping,
- two laser-beam hardening with different angles,
- point two laser-beam hardening with different angles,
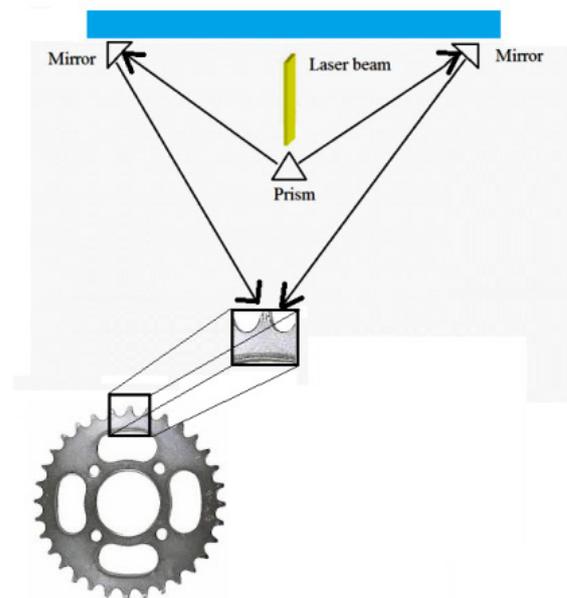- two laser-beam hardening with overlapping with different angles.

ACKNOWLEDGMENT

Fig. 12: Two laser beams in RLH of sprockets.

REFERENCES

[1] Vollertsen, F., K. P., and Meijer, J. State of the art of laser hardening and cladding. In: *Proceedings of the third international WLT-conference on lasers in manufacturing*. Fellbach, Germany: AT-Fachverlag GmbH, 2005.

[2] Frerichs, F., Lu, Y., Lübben, T., and Radel, T. Process signature for laser hardening. *Metals*, Vol. 11, Iss. 3, No. 465, 2021.

[3] Patwa, R., and Shin, Y. C.: Predictive modeling of laser hardening of AISI5150H steels. *International Journal of Machine Tools and Manufacture*, Vol 47, No. 2, pp. 307-320, 2007.

[4] Babič, M.: New double cycle hybrid method of machine learning using laser heat treatment pattern recognition with the topological properties of a network. *Lasers in Engineering*, Vol. 40, No. 1/3, pp. 95-105, 2018.

[5] Iwaszko, J.: Microstructural aspects of laser surface treatment of commercially pure titanium. *Metallic materials,* Vol. 57, No. 1, pp. 11–18, 2019.

[6] Kumar, A. and Kulkarni, G. U.: Evaluating conducting network based transparent electrodes from geometrical considerations. *Journal of Applied Physics*, Vol. 119, No. 1: pp. 015102

[7] Kaplan, A. and Haenlein, M.: Siri, Siri in my Hand, who's the Fairest in the Land? On the Interpretations, Illustrations and Implications of Artificial Intelligence. *Business Horizons*, Vol. 62, pp. 15–25. 2019.

[8] Christopher, C.M.L., Sasikumar, T., Santulli, C., and Fragassa, C.: Neural network prediction of aluminum–silicon carbide tensile strength from acoustic emission rise angle data. *FME Transactions*, Vol. 46, No. 2, pp. 253-258, 2018.

[9] Fragassa, C., Babic, M., Bergmann, C.P., and Minak, G.: Predicting the tensile behaviour of cast alloys by a pattern recognition analysis on experimental data. *Metals,* Vol. 9, No. 557, 2019.

[10] Babič, M., Calì, M., Nazarenko, I., Fragassa, C., et al.: Surface roughness evaluation in hardened materials by pattern recognition using network theory. International Journal on Interactive Design and Manufacturing (*IJIDEM*), Vol. 13, pp. 211-219, 2019

[11] Babič, M., Fragassa, C., Lesiuk, G., Marinković, D.: A new method for complexity determination by using fractals and its applications in material surface characteristics. *International journal for quality research*, Vol. 14, No. 3, pp. 705-712, 2020

[12] Worathep Sae-Long, et al.: Fourth-order strain gradient bar-substrate model with nonlocal and surface effects for the analysis of nanowires embedded in substrate media. *Facta universitatis, Series: Mechanical Engineering*, Vol. 19, No. 4, pp. 657-680, 2021.

[13] Krizhevsky, A., Sutskever, I. and Hinton, G.: ImageNet Classification with Deep Convolutional Neural Networks. In: *Proceedings of NIPS* 2012.

[14] Kovačič, M., Mihevc, A. and Terčelj, M.: Roll wear modeling using genetic programming-industry case study. *Materiali in tehnologije*, Vol. 53, No. 3, pp. 319-325, 2019.

[15] Kovačič, M. and Župerl, U.: Genetic programming in the steelmaking industry. *Genet Program Evolvable,* 2020. https://doi.org/10.1007/s10710-020-09382-5.

[16] Fajfar, I., Puhan, J. and Burmen A.: Evolving a Nelder–Mead Algorithm for Optimization with Genetic Programming. *Evolutionary Computation*, Vol. 25, No. 3, pp. 351-373, 2017.

[17] Pavlovic, A., and Fragassa, C.: Geometry optimization by fem simulation of the automatic changing gear. *Reports in Mechanical Engineering,* Vol. 1, No. 1, pp. 199-205, 2020.

[18] Franulović, M., Marković, K. and Trajkovski, A.: Calibration of material models for the human cervical spine ligament behaviour using a genetic algorithm. *Facta universitatis Series: Mechanical Engineering,* Vol. 19, No 4, pp. 751-765, 2021.

[19] Lacasa, L., Luque, B., Ballesteros, F., Luque, J. and Nuño, J. C.: From time series to complex networks: The visibility graph. In: *Proc. National Academy of Sciences*, Vol. 105, No. 13, pp. 4972–4975.

[20] Mrvar, A. and Batagelj, V.: Analysis and visualization of large networks with program package Pajek. *Complex Adaptive Systems Modeling*, Vol. 4, No. 6, 2016.

[21] Barath Kumar, M.D., Aravindan, K.M., et al: Effect of Post-Fabrication Treatments on Surface Residual Stresses of Additive Manufactured Stainless Steel 316L. *FME Transactions*, Vol. 49, No. 1, pp. 87 – 94, 2021.

[22] Bacciu, D., Errica, F., Micheli, A., and Podda, M.: A gentle introduction to deep learning for graphs. *Neural Networks*, Vol. 129, pp. 203-221, 2020.

[23] Stevanović, I., and Rašuo, B.: Development of a Miniature Robot Based on Experience Inspired by Nature, FME Transactions, Vol. 45, No. 1, pp. 189-197, 2017.

[24] Dulikravich, GS., Martin, TJ., Colaço, MJ., and Inclan EJ.: Automatic switching algorithms in hybrid single-objective optimization, FME Transactions, Vol. 41, No. 3, pp. 167-179, 2013.

МОДЕЛИРАЊЕ ХРАПАВОСТИ ПОВРШИНЕ ЧЕЛИКА НАКОН ЛАСЕРСКОГ КАЉЕЊА КОРИШЋЕЊЕМ 2Д МРЕЖЕ ВИДЉИВОСТИ, КОНВОЛУЦИОНИХ НЕУРОНСКИХ МРЕЖА И ГЕНЕТСКОГ ПРОГРАМИРАЊА

М. Бабич, П. Вангиао, Б. Штер, Д. Маринковић, Ц. Фрагасса

Карактеризација површине материјала након очвршћавања роботом ласером (РЛХ) је технички захтеван поступак. РЛХ се обично користи за очвршћавање делова, посебно када су подложни хабању. Променом њихових површинских својстава, овај третман може понудити неколико предности као што су нижи трошкови за додатну машинску обраду, без употребе расхладних средстава или хемикалија, висока флексибилност, локално очвршћавање, минимална деформација, висока тачност, аутоматизован и интегрисан процес у производном процесу. Међутим, храпавост површине у великој мери зависи од термичке обраде и параметара који се користе у процесу. У овом чланку, приступ теорије мрежа (тј. мрежа видљивости у 2Д простору) је коришћен за анализу храпавости површине алатног челика EH100083-1 на РЛХ. Конкретно, две интелигентне методе су спојене у овој истрази. Прво, генетски алгоритам је примењен да би се извела веза између параметара роботске ласерске ћелије и тополошких својстава површине. Штавише, конволуционе неуронске мреже су омогућиле процену храпавости површине на основу 2Д фотографских слика.